npj climate and atmospheric science

www.nature.com/npjclimatsci

ARTICLE OPEN

Check for updates

Pantropical Indo-Atlantic temperature gradient modulates multi-decadal *AMOC* variability in models and observations

Brady S. Ferster[1,2,7]✉, Leonard F. Borchert[3,4,7]✉, Juliette Mignot[2], Matthew B. Menary[4,6], Christophe Cassou[5] and Alexey V. Fedorov[1,2]

Interconnections between ocean basins are recognized as an important driver of climate variability. Recent modeling evidence suggests that the North Atlantic climate can respond to persistent warming of the tropical Indian Ocean sea surface temperature (SST) relative to the rest of the tropics (*rTIO*). Here, we use observational data to demonstrate that multi-decadal changes in pantropical ocean temperature gradients lead to variations of an SST-based proxy of the Atlantic Meridional Overturning Circulation (*AMOC*). The largest contribution to this temperature gradient-*AMOC* connection comes from gradients between the Indian and Atlantic Oceans. The *rTIO* index yields the strongest connection of this tropical temperature gradient to the *AMOC*. Focusing on the internally generated signal in three observational products reveals that an SST-based *AMOC* proxy index has closely followed low-frequency changes of *rTIO* temperature with about 26-year lag since 1870. Analyzing the pre-industrial control simulations of 44 CMIP6 climate models shows that the *AMOC* proxy index lags simulated mid-latitude *AMOC* variations by 4 ± 4 years. These model simulations reveal the mechanism connecting *AMOC* variations to pantropical ocean temperature gradients at a 27 ± 2 years lag, matching the observed time lag in 28 out of the 44 analyzed models. rTIO temperature changes affect the North Atlantic climate through atmospheric planetary waves, impacting temperature and salinity in the subpolar North Atlantic, which modifies deep convection and ultimately the AMOC. Through this mechanism, observed internal *rTIO* variations can serve as a multi-decadal precursor of *AMOC* changes with important implications for *AMOC* dynamics and predictability.

npj Climate and Atmospheric Science (2023)6:165 ; https://doi.org/10.1038/s41612-023-00489-x

INTRODUCTION

The expected future slowdown of the Atlantic Meridional Overturning Circulation (*AMOC*) in response to anthropogenic climate change can have profound impacts on global and regional climate[1–3]. These impacts include variations of North Atlantic Ocean temperature and changes in its related predictability[1,4], modulation of global air temperature[2,5], regional changes of Northern/Southern hemisphere surface temperature[6,7], changes of storm tracks and associated mid-latitude precipitation[7], alteration of the monsoon systems including Sahelian rainfall[8]. Superimposed modes of North Atlantic sea surface temperature internal variability[9] that are interconnected with *AMOC*[10–13] may mediate some of these impacts[4].

Recent modeling studies have shown that *AMOC* can react to accelerated warming in the tropical Indian Ocean (*TIO*) compared to the rest of the tropics on "fast" (monthly-to-decadal) or "slow" (multidecadal-to-centennial) timescales[14–16]. So far, studies primarily focus on the response of *AMOC* to persistent *TIO* warming, thus targeting potential changes under different levels of global warming and focusing on the Indian Ocean[15]. Variations of *AMOC* in response to internal (i.e., unforced) *TIO* surface temperature variations are unexplored as of yet. Here, we expand on existing research by using observational data sets as well as model simulation ensembles to further illustrate and document *AMOC* response to internal changes of tropical ocean temperature gradients generally and *TIO* more specifically.

Dynamic teleconnections originating from the Tropical Indian Ocean have been shown to influence Arctic and North Atlantic atmospheric patterns (i.e., the Northern Annular Mode & North Atlantic Oscillation, *NAO*)[8,17,18] and atmospheric heat fluxes[19,20] on monthly-to-decadal timescales. The NAO in turn affects both Arctic sea ice[21] and *AMOC*[22] variability. This mechanism is enhanced when relative warming of the TIO compared to the remaining tropics (relative TIO; rTIO) is considered[15].

More recently, such atmospheric pathways have been shown to be complemented by oceanic pathways through the tropical Atlantic[14,15]. *rTIO* warming may drive tropical ocean temperature differences with the Atlantic and Pacific Ocean basins that locally enhances *TIO* precipitation and latent heat release in the atmosphere, inducing a global-scale Gill-type response that involves stationary Rossby and Kelvin waves. This strengthens the Walker circulation across the tropical Atlantic, resulting in increasing wind-induced evaporation and a northward shift of precipitation, ultimately increasing salinity throughout the tropical Atlantic basin. As a result, the tropical ocean temperature gradients related to *rTIO* warming induce positive density anomalies in the tropical Atlantic that are transported through ocean pathways to the North Atlantic and intensify *AMOC* some decades later (further details of the mechanisms e.g., in[14,15]).

The processes by which *AMOC* reacts to changes in anomalous *TIO* temperature have been highlighted in idealized coupled-model sensitivity experiments[14,15] but not yet through observations or free model runs. Further, through their idealized setup, the previous studies targeted forced warming in the *TIO* and its implications for North Atlantic climate[14–16]. This is motivated by the evidence that the *TIO* has warmed by 0.15 °C dec^{-1} and also

[1]Department of Earth and Planetary Sciences, Yale University, New Haven, CT, USA. [2]Sorbonne Universités (SU, CNRS, IRD, MNHN), LOCEAN Laboratory, Institut Pierre Simon Laplace (IPSL), Paris, France. [3]Center for Earth System Research and Sustainability CEN, Universität Hamburg, Hamburg, Germany. [4]Laboratoire de Météorologie Dynamique (LMD), École Normale Supérieure (ENS), Paris, France. [5]CERFACS, Toulouse, France. [6]Present address: Met Office Hadley Centre, Exeter, UK. [7]These authors contributed equally: Brady S. Ferster, Leonard F. Borchert. ✉email: brady.ferster@locean.ipsl.fr; leonard.borchert@uni-hamburg.de

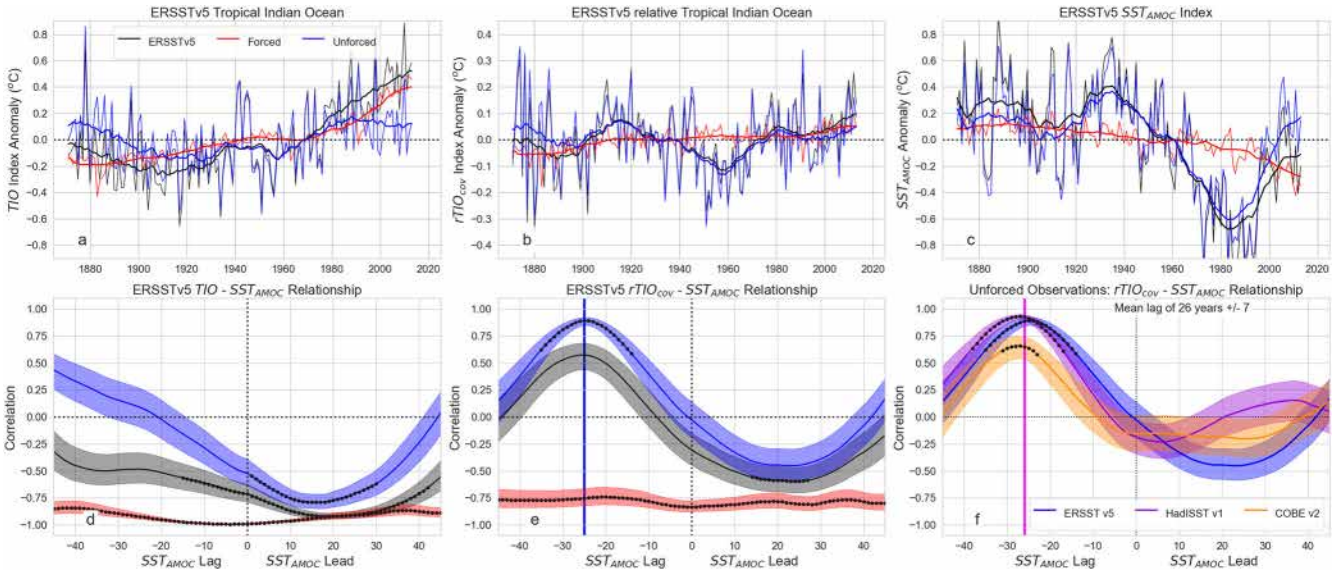

Fig. 1 Temperature time series for the Tropical Indian Ocean and the SST_{AMOC} index, as well as their cross-correlations in reanalysis data sets. Time series of the observed ERSST (black) and decomposed into the forced (red) and unforced internal (blue) components for the (**a**) tropical Indian Ocean (TIO) sea surface temperature (SST), (**b**) relative tropical Indian Ocean SST weighted by covariances ($rTIO_{cov}$), and (**c**) *AMOC* SST-fingerprint index SST_{AMOC}. Thin lines represent the annual mean and the thick line the 21-year moving mean. **d**, **e** The lag-lead correlations of *TIO* and $rTIO_{cov}$ with the SST_{AMOC} for the observed (black), forced (red), and unforced (blue) filtered ERSST time series, respectively. The vertical blue line represents the time-lag of the peak correlation of the unforced signal (**e**). **f** The lag-lead correlation between the $rTIO_{cov}$ and SST_{AMOC} unforced indices for ERSST v5 (blue), HadiSST v1 (purple), and COBE v2 (orange). The vertical magenta line represents the mean of the maximum correlations between the three observational indices, the shading represents the 95% confidence interval of upper and lower bound uncertainty, and black dots highlight correlation significantly different from 0 at the 95% confidence level based on a Student's *t* test and according for smoothing (see Methods). The years used for each observational data product is from 1871 to 2013.

experienced enhanced warming of 0.05 °C dec^{-1} compared to the rest of the tropics since 1960[14]. However, there was no detailed breakdown of the involved tropical ocean temperature gradients to the diagnosed *rTIO-AMOC* connection. In addition, unforced internal climate variations are important to understand global teleconnections and to forecast near-term climate variations on the decadal time scales and the associated impacts[23,24] beyond the previously studied forced *rTIO*-driven *AMOC* intensification. Specifically, understanding and accounting for internal variability in the North Atlantic has been shown to be a potent tool in the attempt to predict climate over the adjacent continents on the seasonal-to-decadal time scales[2,25,26]. Since some modes of tropical Indian Ocean *SST* variability exhibit pronounced multi-annual variations[27] which carry some decadal predictability[28], the *rTIO-AMOC* link is a promising mechanism to better understand *AMOC* variations and predictability.

In this work, we examine internal *rTIO-AMOC* teleconnections diagnosed from observational data sets, following the methods of previous literature, to show how the two ocean basins are interconnected. We also take the opportunity to "zoom out", analyzing in detail which ocean regions and tropical ocean basins contribute to the tropical temperature gradients that govern the *rTIO-AMOC* mechanisms from the literature. We then analyze model simulations to understand the robustness of the internal *rTIO-AMOC* connection. Finally, we draw conclusions on the importance of these internal mechanisms in the face of anthropogenic global warming, offering alternative interpretations of *SST*-based observed *AMOC* fingerprints in the context of internal variability.

RESULTS

Observed tropical ocean SST teleconnections to AMOC

Direct observation of the influence of tropical ocean temperature gradients on *AMOC* is inhibited by a lack of long-term direct *AMOC* observations[29,30]. In this context, a North Atlantic *SST* index was proposed as a proxy for *AMOC* fluctuations[10,31]. This index is defined as the mean extended winter (November-May: NDJFMAM) difference between North Atlantic subpolar gyre and global mean *SST*[31]. It projects onto the annual mean *AMOC*[31]. Since *SST* has been observed and reconstructed for much longer than *AMOC*, we here invoke this observed SST-based *AMOC* index (henceforth *SST AMOC index;* SST_{AMOC}) to reconstruct *AMOC* variations and examine the tropical ocean—*AMOC* teleconnection mechanism in observational data sets. Furthermore, the objective of this study is to investigate the internal variability, separate from the anthropogenic forced signal. We separate the forced component from unforced internal climate variability using the residuals method that subtracts the multi-model ensemble mean of historical simulations from observations (see Methods)[32] to focus on unforced effects. To this end, we estimate the forced signals from CMIP6 historical simulations (see *Methods*)[32–34]. Unless explicitly stated otherwise, the results we describe henceforth will be interpreted as unforced residuals, i.e., internal variability.

Continuing from previous literature[14,15], we first define a $rTIO_{cov}$ index. We define this index as the *TIO* temperature minus the remaining tropical ocean temperature, weighted by its covariance with *TIO* temperature ($TIO\text{-}TO_{cov}$, see *Methods*). Compared to the previous method, we thus now account for the co-variability between the indian ocean and the other tropical basins to focus on the signal related to the TIO and reduce contamination of our results from other decadal-to-multi-decadal climatic modes.

The full observed *TIO*, $rTIO_{cov}$ and SST_{AMOC} all display pronounced decadal-scale variability, as well as an accelerating trend over the later decades due to external forcing of the climate system (Fig. 1a–c). This includes both the unforced internal and the forced signal. A trough and peak are observed in 1890 and 1910 in $rTIO_{cov}$, and in 1910 and 1930 in SST_{AMOC}. We find a temperature drop and subsequent recovery between 1920 and 1960 in $rTIO_{cov}$ and a substantial drop between 1940 and 1980 in

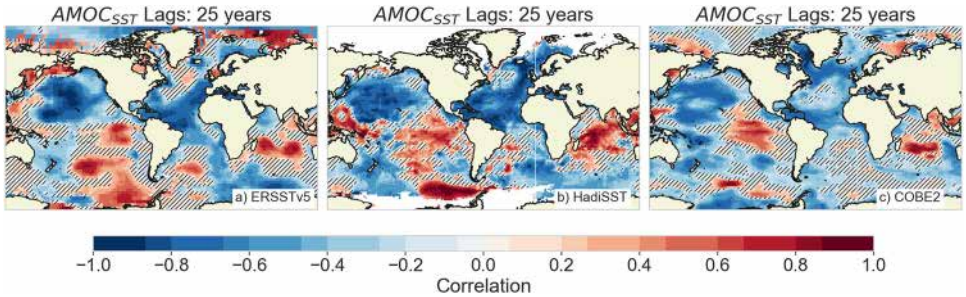

Fig. 2 Correlations between the *AMOC* SST-fingerprint index SST_{AMOC} and SST fields, when SST leads SST_{AMOC} by 25 years, for the unforced signal in ERSST v5, HadiSST v1, and COBE v2. For each correlation, the time period 1871–2013 was used with a 21-year moving mean applied. A 25-year lag was selected based on the results in Fig. 1 and similar spatial patterns result when changing the lag time by ±5 years due to applying a 21-year moving mean to identify the low frequency signal. Hatching represents those spatial correlations that are not significant at the 95% confidence interval, taking into account the smoothing and autocorrelation.

SST_{AMOC}. The observed *TIO* and $rTIO_{cov}$ indices show a significant negative correlation with SST_{AMOC} when the latter leads by approximately 20 years (Fig. 1d, e; $r = -0.92$ and -0.60 respectively, solid black).

To improve our understanding of the underlying connections, we deconstruct the observed signal into a forced (red) and an unforced (blue) component. The forced *TIO* and $rTIO_{cov}$ signal are steadily warming, while forced SST_{AMOC} cools. The latter suggests *AMOC* weakening over time (red lines in Fig. 1a–c) related to anthropogenic climate change (as also argued in[31]). It is worth noting that, as estimated from the SST_{AMOC} proxy with forcing estimation from climate models, this study cannot make any statements about the emergence of *AMOC* weakening in observations. The unforced signal of *TIO* and SST_{AMOC} have a negative correlation maximum when the *TIO* lags by 17 years (Fig. 1d, solid blue, $r = -0.80$) and the modulations of $rTIO_{cov}$ and SST_{AMOC} have a positive correlation maximum when $rTIO_{cov}$ leads by 25 years (Fig. 1e, solid blue, $r = 0.89$). We do not find a significant correlation between the $rTIO_{cov}$-SST_{AMOC} at short time lags, indicating that the mechanism that dominates the unforced signal in observations acts on multidecadal time scales.

The multidecadal relationship with $rTIO_{cov}$ leading *AMOC* is robust when considering sub-periods of the time series (Supplementary Fig. 1), indicating that it is a robust relationship that is not just dominated by the large drop in the *SST* time series around the 1960s. The time scale of some 25 years aligns with published estimates of a dynamic $rTIO_{cov}$-*AMOC* pathway in climate models[14,18,35]. It therefore seems that the $rTIO_{cov}$-*AMOC* connection is not only a forced response, as suggested by previous studies, but also a feature of unforced variability.

The decomposition of the relationship between $rTIO_{cov}$ and SST_{AMOC} shown here with ERSST v5[36] is robust in HadiSST v1[37] ($r = 0.93$, 27 years) and COBE v2[38] ($r = 0.66$, 27 years) (Fig. 1f and S1), with an average positive correlation maximum when the unforced $rTIO_{cov}$ leads by 26 ± 7 years (mean ± 99% confidence interval). Since the relationship of $rTIO_{cov}$ and SST_{AMOC} in response to global warming is opposite in sign, but the unforced correlation shows the described positive maximum (Fig. 1c) with some lags, processes involved in internal variability are likely different from those related to anthropogenic forcing, which warrants further exploration.

To better understand the tropical temperature gradients that precondition the influence of $rTIO_{cov}$ on *AMOC*, we set aside the proposed $rTIO_{cov}$ index and propose to further understand spatial patterns of the tropical temperature gradients using a lagged correlation analysis (Fig. 2). Observations show significant positive tropical SST correlation to SST_{AMOC} in the *TIO* and tropical eastern Pacific Ocean when tropical SST leads by more than 20 years. The tropical Atlantic Ocean (*TAO*) is significantly negatively correlated to SST_{AMOC} at the same time lag. This suggests that a tropical *SST* gradient involving the Indian and eastern Pacific (*IEP*) on the one hand, and the Atlantic on the other hand, may induce the slow mechanism. These patterns are robust across all three observational products and several time lags (not shown). We exclude the tropical western Pacific as it shows no robust pattern amongst the three observed products. From the identified *IEP-TAO-TIO* pattern, we can construct alternate indices of tropical SST gradients defined as the *IEP* minus the *TAO* weighted by their covariance (*IEP-TAO*$_{cov}$). *TIO-TAO*$_{cov}$ and *EP-TAO*$_{cov}$. These indices are examined to identify a potential dominance of one the tropical basins linking to SST_{AMOC}. Comparing the proposed tropical *SST* gradient metrics with the $rTIO_{cov}$ (Supplementary Fig. 2), the strongest correlations with SST_{AMOC} are still found with the $rTIO_{cov}$ approach (*TIO-TO*$_{cov}$). Within the TG_{SST} metrics, the *TIO-TAO*$_{cov}$ produces the highest correlations while the *EP-TAO*$_{cov}$ the lowest of the three within all three sets of observational products (Supplementary Fig. 3). Although the spatial pattern suggests an *IEP-TAO* relationship (Supplementary Fig. 3), this analysis suggests the importance of the *TIO* and *TAO* in determining the TG_{SST} with potentially less importance of the *EP*. Yet, due to the overall highest and most consistent correlations of the $rTIO_{cov}$ with SST_{AMOC} among the tropical ocean temperature gradient indices in all three observations, we henceforth define the $rTIO_{cov}$ index as *TIO-TO*$_{cov}$ for comparison within coupled models (see *Methods* and Supplementary Fig. 2). To further understand its robustness and underlying processes, we now investigate the internal $rTIO_{cov}$-*AMOC* relationship in climate model simulations in the absence of forcing.

Unforced rTIO-AMOC connections in models

We examine pre-industrial control (piControl) simulations from 44 different models from the Coupled Model Intercomparison Project Phase 6 (CMIP6)[39] archive. This kind of model simulation allows assessing climate variability due to internal processes only, as external forcings are kept constant to their 1850 estimated values. As in the analysis of observations, we analyze low-pass filtered model output. To account for smoothing-related end-point effects, we do not analyze the first or last 100 years of the simulations. The examined CMIP6 simulations produce a $rTIO_{cov}$-SST_{AMOC} correlation maximum at 26 ± 6 years (99% confidence interval, Fig. 3), with a subset of 28 out of the 44 CMIP6 models within the observed estimate of 26 ± 7 years. In fact, the time lag in the CMIP6 model subset is on average 27 ± 2 years and shows a significant multi-model correlation maximum ($r = 0.50$) within the observed time lag (Fig. 3a; see Supplementary Table 1). The majority of models thus confirms the observed internal correlation. We now examine this subset of models more closely.

Climate model simulations have the benefit of providing complete information about the (simulated) climate system, so that the actual *AMOC* can be diagnosed. We find that the

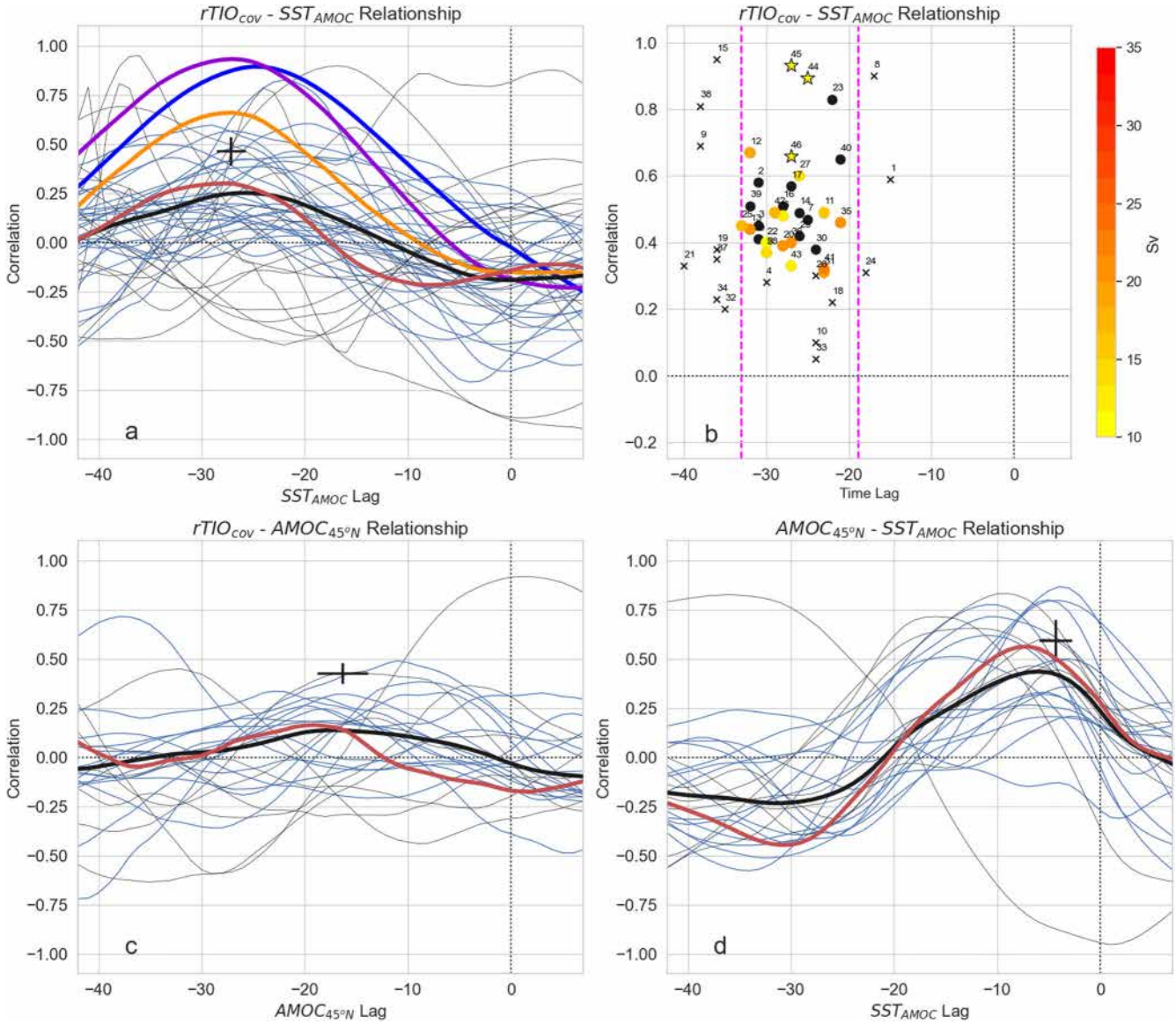

Fig. 3 The relationship between *rTIO$_{cov}$* and *SST$_{AMOC}$* in the CMIP6 model archive. Correlations of (**a**) *rTIO$_{cov}$*-*SST$_{AMOC}$* across different time lags for observations from Fig. 2 (thick blue, purple and yellow lines) and the different CMIP6 model pre-industrial control simulations. Those models that show a correlation maximum greater than the 0.30 threshold from bootstrapping and within 99% confidence interval of the observed *rTIO$_{cov}$*-*SST$_{AMOC}$* lag of 26 years are shown in thin blue lines (CMIP6 subset), while those in thin gray are those outside the observed range. The thick red line represents the IPSL-CM6A-LR model shown in more detail in Fig. 4 and the thick black line is the CMIP6 subset model mean, both estimated using Fisher's Z-transformation. **b** A scatter plot of the maximum *rTIO$_{cov}$*-*SST$_{AMOC}$* correlation and time lag for the mean relationship in each CMIP6 model. Those of the CMIP6 subset are plotted in circles and those not in the subset are denoted with an "x". The colorbar depicts mean *AMOC* strength at 45 °N within the model, which is only available for a few of the subset models and the 3 standard deviation thresholds are denoted with dashed magenta lines. The observed ERSST v5, HadiSST v1, and COBE v2 correlations are denoted with yellow stars within (**b**). A complete list of the corresponding models can be found in Supplementary Table 1. **c**, **d** as (**a**), but for *rTIO$_{cov}$*-*AMOC$_{45N}$* and *AMOC$_{45N}$*-*SST$_{AMOC}$*, respectively. The thick black line indicates the mean correlation value across all models. Potential temporal offsets between correlation maxima are reflected in the black error bars, which represent the mean correlation value, mean maximum correlation time lag, and the respective 1–99% confidence intervals of the correlation peaks identified in each of the CMIP6 models using Fisher's Z-transformation.

aforementioned subset of models (28 of 44) also shows on average positive correlation between *rTIO$_{cov}$* and *AMOC* at 45°N (*AMOC$_{45N}$*) when *rTIO$_{cov}$* leads by 17 ± 5 years ($r = 0.43$) (Fig. 3a–c). The observed ERSST value of $r = 0.89$ lies in the highest decile of the model correlation values (Fig. 3b). The *AMOC$_{45N}$* and *SST$_{AMOC}$* relationship is very robust in this subset of CMIP6 piControl simulations: their average correlation is 0.60 when *AMOC$_{45N}$* leads by 4 ± 3 years (Fig. 3d). At lower latitudes the *AMOC* lead becomes shorter (e.g., *AMOC$_{26N}$* shows a maximum correlation to *SST$_{AMOC}$* at 2 ± 3 years, $r = 0.80$; not shown), illustrating the *AMOC* dynamics of subsurface southward propagation of *AMOC* anomalies[11] and surface features represented by *SST$_{AMOC}$*. Overall, these findings highlight the robustness of the *SST$_{AMOC}$* fingerprint for estimating *AMOC*.

The low correlation values in models compared to observations can be partly attributed to the length of time series. The 44 piControl simulations have a length of between 300 and 2000 years, and therefore represent a multitude of possible climatic states or regimes, not all of which are necessarily representative of the relatively short observed period. In each model, we thus

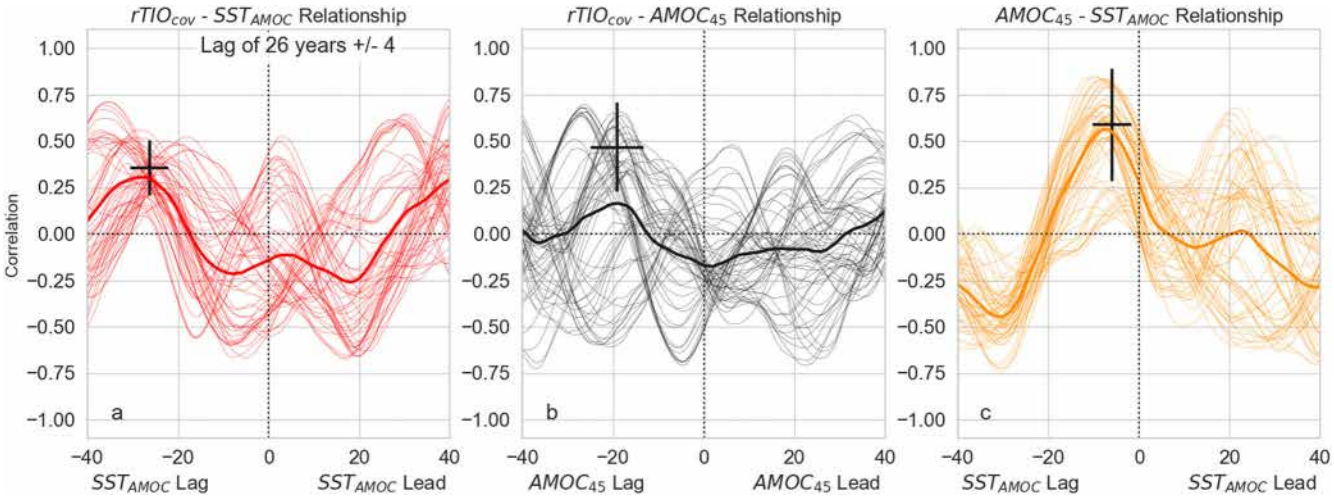

Fig. 4 A detailed view of the *rTIO$_{cov}$-AMOC* relationship in the IPSL-CM6A-LR model. Lag-lead correlations between the (**a**) *rTIO$_{cov}$-SST$_{AMOC}$* (red), (**b**) *rTIO$_{cov}$-AMOC$_{45N}$* (black), and (**c**) the *AMOC-SST$_{AMOC}$* (blue) indices in the IPSL-CM6A-LR piControl simulation. The thin lines represent individual 150-year segments, and the thick lines are the mean correlations of all segments, estimated from a Fisher's Z-transformation. The crosses/error bars represent the standard deviation of the maximum correlation lag in all 150-year long segments of the 1200-year piControl run for correlations between the three different indices. The black error bars represent the approximate mean correlation and the respective 99% confidence interval of the maximum correlation lag in all 150-year long segments of the 1200-year piControl run for correlations between the three different indices.

consider the 150-year long slices of the piControl simulations that show the maximum *rTIO$_{cov}$-SST$_{AMOC}$* correlation within the observed time lag to mimic the length of the observational period (Fig. S3). 31 of 44 (~70%) models show time slices that lie within the observed time lag estimate of the *rTIO$_{cov}$-SST$_{AMOC}$* relationship. In this analysis, the CMIP6 average maximum correlation values (black error bars in Fig. S3) of *rTIO$_{cov}$-SST$_{AMOC}$*, *rTIO$_{cov}$-AMOC$_{45N}$*, and *AMOC$_{45N}$-SST$_{AMOC}$* are 0.65 at 26 ± 2 years lag, 0.67 at 19 ± 6 years lag, and 0.81 at 7 ± 4 years lag, respectively. We find that most of the examined CMIP6 models are capable of reproducing the observed unforced *rTIO-SST$_{AMOC}$* relationship in at least one 150-year time slice. Yet, while the *SST$_{AMOC}$-AMOC$_{45N}$* relationship is found to be robust as well, the *rTIO$_{cov}$-AMOC$_{45N}$* relationship is not coherent across all models, probably due to non-linearities and competing effects in the relationships.

We detail the specificities of the proposed *rTIO-AMOC* link in the most recent version of the IPSL climate model, the IPSL-CM6A-LR model (Fig. 4)[40]. In agreement with observations and the majority of examined CMIP6 models, the IPSL-CM6A piControl simulation shows a *rTIO$_{cov}$-SST$_{AMOC}$* correlation peak when *rTIO$_{cov}$* leads by 26 ± 4 years (Fig. 4a). This average peak is much lower than observed (0.36 vs. 0.89 in ERSST), yet significant. In 150-year long slices of the piControl simulation, the intermittent *rTIO-SST$_{AMOC}$* correlations reach values of up to 0.56 and a standard deviation of 0.12 between the slices when *rTIO$_{cov}$* leads by 26 ± 4 years (Figs. 4, S4, S5). Moreover, values can approach correlations of 0.71 within IPSL-CM6A-LR, although occurring when lags are >33-years and exceeding the threshold based on the observed products, suggesting a potential relationship to modeled mean AMOC strength in determining the lag.

The 1200-yr long IPSL-CM6A-LR simulation shows a significant correlation ($r = 0.59$) between *SST$_{AMOC}$* and *AMOC$_{45N}$* when *AMOC$_{45N}$* leads by 6 years (Fig. 4b). Correlation between *rTIO$_{cov}$* and *AMOC$_{45N}$* is significant ($r = 0.46$) when *rTIO$_{cov}$* leads by 19 years. These time lags align with those in observations and CMIP6 models. In 150 year time slices, the maximum correlation between *rTIO$_{cov}$* and *AMOC$_{45N}$* is 0.70 (standard deviation between time slices = 0.20) when *rTIO$_{cov}$* leads by 19 ± 2 years. We find a similar spread between time slices in *AMOC$_{45N}$ - SST$_{AMOC}$* correlations ($r = 0.70$, standard deviation = 0.12) when *AMOC$_{45N}$* leads by 6 ± 2 years (Fig. 4c). As a result, the internal relationship between *rTIO$_{cov}$* temperature and *AMOC$_{45N}$* in IPSL-CM6A-LR is weak and intermittent, but robust when *rTIO$_{cov}$* leads by roughly 20 years.

The spatial signal of rTIO-AMOC connections

We now examine the physical pathways that connect the tropical ocean temperature gradient to *SST$_{AMOC}$* in the IPSL-CM6A-LR climate model. *rTIO$_{cov}$* warming enhances geostationary Rossby wave generation in the *TIO* region through enhanced precipitation and latent heat release[18,41], simultaneously driving a negative NAO-like pressure pattern in the North Atlantic alongside a southward shift in zonal wind stress over the subpolar Atlantic and an adjustment of meridional wind stress (Supplementary Fig. 5a–d). Ekman pumping in the subpolar North Atlantic responds to the atmospheric anomalies by increasing in magnitude, resulting in warmer, saltier, and denser waters (Supplementary Fig. 5e–h) within the eastern subpolar North Atlantic and deep convective regions. These climatic conditions persist for 10–15 years (Supplementary Fig. 6), demonstrating the low-frequency patterns in phase with the *rTIO* as also shown by[35]. Such prolonged *NAO* conditions impact *AMOC*, leading to changes in the entire water column (Supplementary Fig. 7) and southward propagation of an *AMOC* anomaly after 20 years (Supplementary Fig. 8)[35]. This *AMOC* anomaly feeds back onto *SST*, influencing the *SST$_{AMOC}$* index at a time lag of around 5 years (Supplementary Fig. 6f), which explains the overall observed and simulated time lag between *rTIO$_{cov}$* and *SST$_{AMOC}$*, and explains differences in lags of the *rTIO$_{cov}$* and *AMOC$_{45N}$* (~19 years) and *SST$_{AMOC}$* (~26 years) in the IPSL model (Fig. 4) which we also demonstrated with CMIP6 (Figs. 3, S3).

Although some of our findings show characteristics of an alternative mechanism that describes a *rTIO* influence on the *TAO*[42] and a propagation of that signal into the subpolar North Atlantic, we fail to clearly diagnose this mechanism in this work. This suggests that the direct connection to the North Atlantic via the *NAO* dominates the internal influence of *rTIO$_{cov}$* on *AMOC*.

DISCUSSION

A key assumption of this work is the use of the SST-based *SST$_{AMOC}$* index to estimate observed internal *AMOC* changes. This index has

been designed to describe the full *AMOC* modulations and trends, but its suitability for addressing internal *AMOC* variations had to our knowledge not been assessed. Debates continue on the extent to which this index describes forced[31] vs. internal atmospheric variability[43] in the observed record. Using CMIP6 model simulations, we here show that there is overwhelming model agreement on the unforced internal correlation of SST_{AMOC} and $AMOC_{45N}$ when $AMOC_{45N}$ leads by around 6 years (Fig. 3d; as also suggested by[44]). The 150-year long time chunks in CMIP6 piControl simulations encompass correlation values of 0.60 ± 0.27 (0.81 ± 0.37 for the 44 best 150-year chunks), indicating that the use of the SST_{AMOC} index to assess internal fluctuations of $AMOC_{45N}$ is justified.

As discussed further up, various tropical ocean temperature gradients could have been chosen to be examined for their influence on *AMOC* in this study (cf. surface temperature patterns in Fig. 2). Comparing the observed influence of different options (Supplementary Fig. 2) we found that all selected indices show comparable results. Here, we chose to focus on $rTIO_{cov}$ due to its highest correlation to SST_{AMOC}, and because of its presence in published literature. The $rTIO_{cov}$ index is considered here to be representative of all examined tropical ocean temperature gradients, and our results are robust across these definitions of tropical ocean temperature gradients (Figs. 1, 2, S2, S3, and S5). Other indices potentially contribute to AMOC modulation through teleconnections, and further work is necessary to derive the exact mechanisms at work.

Our work assumes that the CMIP6 multi-model mean of historical simulations appropriately estimates the forced response of the observed climate system. Results presented here are robust to using the IPSL model single model ensemble mean instead of the multi-model mean for the forced response (Supplementary Fig. 9a, b), thereby giving credit to the assumption that an ensemble mean of historical simulations is a relevant estimation of the effect of external forcing on climatic variables. While models may not appropriately represent the response of the climate to forcing, which is a clear limitation to any study examining climate model ensemble averages, the CMIP6 historical simulations are the best available estimate of the forced response of the climate system at this time which, unlike statistical detrending, accounts for abrupt climate events such as volcanic eruptions or aerosol concentration changes. That being said, some evidence of powerful statistical detrending methods exist[45], which go beyond what can be covered in this paper.

As we find the $rTIO_{cov}$-AMOC relationship in about 60% of the CMIP6 historical members—a corresponding analysis using only the IPSL model historical ensemble, subtracting the IPSL ensemble mean to remove the forced response, shows comparative results (19/33 members reproduce the mechanism) –, this illustrates both that it is the dominant mechanism in these models and that it is inherently intermittent. Such intermittency is consistent with[46]. An analysis of the intermittency of the relationships of $rTIO_{cov}$, SST_{AMOC} and $AMOC_{45N}$ (Figs. 4, S4) across the IPSL piControl simulation illustrates that the $rTIO_{cov}$-$AMOC_{45N}$ relationship breaks down when the $AMOC_{45N}$-SST_{AMOC} relationship decreases, while the teleconnection between $rTIO_{cov}$ and the SST_{AMOC} remains relatively stable. This implies changes in the North Atlantic climate, potentially related to NAO, that break down the $AMOC_{45N}$-SST_{AMOC} relationship as probable causes of the intermittency in the $rTIO_{cov}$-$AMOC_{45N}$ relationship[46], while the interbasin atmospheric teleconnection remains intact.

Only a subset of CMIP6 models appear to consistently reproduce the observed internal $rTIO_{cov}$-SST_{AMOC} relationship. Here, the non-stationarity of the relationship could be one possible reason, as the examined simulations cover different time lengths, and differences in the surface and subsurface features could differ in the different periods examined. Another potential reason is that some models might not capture the teleconnection mechanism due to coarse resolution, mean biases, the signal to noise problem in global climate models[47], issues with mixing in the North Atlantic in some models[48], or missing representation of the stratosphere which is crucial to simulating atmospheric waves[49], along many other possible reasons. Alternative interpretations of this caveat are that the observed $rTIO_{cov}$-SST_{AMOC} relationship is spurious in observations and erroneously reproduced by some climate models. Model differences that cause these discrepancies in the $rTIO_{cov}$-$AMOC_{45N}$ mechanism will be important to study in future research.

This work could not clearly separate the influence of $rTIO_{cov}$ on $AMOC_{45N}$ from other factors influencing the $AMOC_{45N}$ internal variability. Given the relatively short observational record, the $rTIO_{cov}$ connection of *AMOC* might well be related to known interbasin teleconnections[50], part of a self-containing mechanism of *AMOC* variability[51] or another teleconnection via the NAO[18,35,52]. However, this study implies a tropical SST gradient as a potentially important driver or at least pacemaker of *AMOC* changes, identifying additional TG_{SST} indices that strongly rely on the variability of the tropical Indian and Atlantic Oceans. Disentangling the different drivers of *AMOC* variability is an exciting scientific question for the future.To conclude, we have analyzed several observational data sets as well as global climate model simulations from the CMIP6 archive to establish a pathway by which low-frequency internal, i.e., unforced, changes of tropical ocean temperature gradients may influence *AMOC* several decades later, leading to *AMOC* multi-decadal variability. This pathway includes shifts in geostationary waves that impact the NAO, changing surface winds with impacts on salinity and temperature distributions that change Ekman pumping, impacting *AMOC*. In models, internal $rTIO_{cov}$ warming strengthens *AMOC* ~ 20 years later. We also find that across model simulations a SST-based index that was proposed to indicate forced *AMOC* changes[10,31] is reflective of internal *AMOC* changes ~6 years earlier, allowing a tracking of *AMOC* changes using relatively easily observable surface water characteristics. This study implies that $rTIO_{cov}$ temperature is an important pacemaker of *AMOC* variability as well as a potential early warning indicator of multi-decadal *AMOC* change.

METHODS

Observations

As one estimate of observational uncertainty, we analyze the gridded observational data sets/reanalysis products ERSST v5[36], HadiSST v1.1[37], and COBE v2[38] for the period 1870–2014. All gridded products are regridded to a regular 1 × 1 degree grid prior to analysis, and anomalies to their respective long-term mean states are formed.

Models

We detail the mechanisms discussed in this paper in two different model setups. To find the response of the climate system to forcing, we analyze a 44-model ensemble-mean of historical simulations from CMIP6[39]. The models are detailed in Supplementary Table 1. Prior to forming the multi-model mean, individual model ensemble means are calculated (i.e., we follow the one-model-one-vote approach[53]), regridded to a regular 1 × 1 degree grid, and then anomalies to their mean state formed to account for model mean bias. These model simulations are all characterized by the same forcing but utilizing different model setups and different initial conditions. The multi-model mean can therefore be regarded as a "best estimate" of the forced response of the system.

We also analyze the unforced physical pathways that connect Indian Ocean SST to the North Atlantic and *AMOC* in pre-industrial control simulations with the same GCMs (Supplementary Table 1). These model simulations are not subject to forcing and therefore represent the respective model's interpretation of internal climate

variability. Some CMIP6 GCMs show a pronounced centennial fluctuation in global SST, which may project onto local SST variability[40]. To account for this, we high-pass filter all model output that we analyze at a 100-year cut-off frequency.

METHODS

In this paper, we analyze annual and boreal extended winter (November-May, NDJFMAM) mean SST, SSS, precipitation, evaporation minus precipitation and 500 hPa geopotential height and annual meridional overturning streamfunction, which are then—unless otherwise noted—low-pass filtered with a 21-year running mean. Two specific indices are considered in our analysis. First, we average annual mean SST in the tropical Indian Ocean (30° S–30° N, 40° W–100° W), and then subtract SST in the remaining Tropics (*TO*; 30° S–30° N) multiplied by the weighted covariances between the two to calculate the $rTIO_{cov}$ index, similar to[14,15] but now accounting for the covariances of the tropical Indian SST modulations with the rest of the tropical ocean. This is illustrated in Eq. (1):

$$\mathrm{rTIO_{cov}} = \mathrm{TIO} - \left(\mathrm{TO} \times \frac{\mathrm{cov(TIO, TO)}}{\mathrm{cov(TO, TO)}}\right) \quad (1)$$

Other tropical basins similarly use 30° S–30° N as boundaries for the tropics and the *EP* is defined from 150 °E to 80 °E. As shown in Figs. 2 and S1, there are several tropical regions that could demonstrate a tropical gradient that relates to the SST_{AMOC}. We have chosen to define the $rTIO_{cov}$ as the gradient between the *TIO* and *TO* because of its use in previous literature, and because in observations we find the highest correlation to SST_{AMOC} when comparing with other indices for tropical temperature gradients (Supplementary Fig. 1). Several additional gradients that are based on the tropical Indian and Atlantic Oceans suggest that the potential key interactions rely on these two basins, with some influence from the tropical East Pacific. Second, in the face of a shortage of *AMOC* observations that go back in time further than 2005, we calculate the *AMOC* SST-fingerprint following the methods proposed in[10,31] as a proxy. This SST_{AMOC} index is calculated by subtracting winter global mean SST (60° S–70° N) from subpolar North Atlantic winter *SST*, as defined in[31], but the idea of a *SST* fingerprint of *AMOC* has been similarly been described previously[11,54,55].

There are numerous approaches in the literature to remove the forced signal from models and observations[32–34]. We here analyze observed unforced climate variability, calculated following the "residuals"-approach[32]. This technique rescales the historical multi-model ensemble mean variability to the observed value in order to estimate the forced component using the ratio of observed and multi-model mean standard deviations[32], and then subtracts on a grid-point basis the forced component from the full signal. The residual signal is treated as observed unforced internal variability in this study[26]. To compare correlations between the various temperature and *AMOC* indices in the models, the simulations are first high-pass filtered using a Butterworth filter of a 100-year cut-off frequency to remove a known 100-year centennial mode[40], and then smoothed using a 21-year moving mean to remain consistent between the methods of the SST_{AMOC} and the other indices. Pearson correlation analysis is performed at different temporal lags to find statistical relationships between variables and tested for statistical significance using a bootstrapping of 1000 iterations and an alpha of 0.05. Given 11 years of diagnosed significant autocorrelation in the filtered time series (not shown), we account for autocorrelation by bootstrapping the data by blocks of 11 years. Given the sample size, significance threshold, and accounting for autocorrelation, the threshold of a significant correlation at a lag of 26 years (chosen from the observed lag) is 0.30. To help compare the lag-lead correlations of the indices, we transform them from a logarithmic to a linear scale using a Fisher's Z transform to average correlations. However, the lag-lead correlation values vary in time and magnitude with index comparisons. To find the mean correlation of a lag-lead relationship, we identify the time of maximum peak or trough of the signal and use the Fisher's Z transformation on the peaks/troughs to average the transformed correlation values centered around the maximum/minimum correlation.

DATA AVAILABILITY

The data that support the findings of this study are all available within the data repositories detailed below. The defined subpolar North Atlantic region from Caesar et al., 2019 is available from http://www.pik-potsdam.de/~caesar/AMOC_slowdown/. The HadiSST data set is available at Met Office, Hadley Centre (https://www.metoffice.gov.uk/hadobs/hadisst/). The COBE SST and NOAA ERSST data sets are available at NOAA Earth System Research Laboratory's Physical Sciences Division (https://www.esrl.noaa.gov/psd/data/gridded/data.cobe.html; https://www.esrl.noaa.gov/psd/data/gridded/data.noaa.ersst.v5.html). Information for CMIP6 data is available from the World Climate Research Programme (WCRP) webpage (https://esgf-index1.ceda.ac.uk/projects/cmip6-ceda/) and the data for this experiment is archived on the IPSL cluster in Paris, France (https://esgf-node.ipsl.upmc.fr/search/cmip6-ipsl/).

Received: 30 September 2022; Accepted: 25 September 2023;
Published online: 19 October 2023

REFERENCES

1. Liu, W., Fedorov, A. V., Xie, S.-P. & Hu, S. Climate impacts of a weakened Atlantic Meridional Overturning Circulation in a warming climate. *Sci. Adv.* **6**, eaaz4876 (2020).
2. Bonnet, R. et al. Increased risk of near term global warming due to a recent AMOC weakening. *Nat. Commun.* **12**, 6108 (2021).
3. An, S. et al. Global Cooling Hiatus Driven by an AMOC Overshoot in a Carbon Dioxide Removal Scenario. *Earths Future* **9**, e2021EF002165 (2021).
4. Borchert, L. F., Müller, W. A. & Baehr, J. Atlantic Ocean Heat Transport Influences Interannual-to-Decadal Surface Temperature Predictability in the North Atlantic Region. *J. Clim.* **31**, 6763–6782 (2018).
5. Caesar, L., Rahmstorf, S. & Feulner, G. On the relationship between Atlantic meridional overturning circulation slowdown and global surface warming. *Environ. Res. Lett.* **15**, 024003 (2020).
6. Vellinga, M. & Wood, R. A. Global Climatic Impacts of a Collapse of the Atlantic Thermohaline Circulation. *Clim. Change* **54**, 251–267 (2002).
7. Jackson, L. C. et al. Global and European climate impacts of a slowdown of the AMOC in a high resolution GCM. *Clim. Dyn.* **45**, 3299–3316 (2015).
8. Bader, J. & Latif, M. North Atlantic Oscillation Response to Anomalous Indian Ocean SST in a Coupled GCM. *J. Clim.* **18**, 5382–5389 (2005).
9. Delworth, T. L. et al. The Central Role of Ocean Dynamics in Connecting the North Atlantic Oscillation to the Extratropical Component of the Atlantic Multidecadal Oscillation. *J. Clim.* **30**, 3789–3805 (2017).
10. Zhang, R. Coherent surface-subsurface fingerprint of the Atlantic meridional overturning circulation. *Geophys. Res. Lett.* **35**, L20705 (2008).
11. Zhang, J. & Zhang, R. On the evolution of Atlantic Meridional Overturning Circulation Fingerprint and implications for decadal predictability in the North Atlantic. *Geophys. Res. Lett.* **42**, 5419–5426 (2015).
12. Oelsmann, J., Borchert, L., Hand, R., Baehr, J. & Jungclaus, J. H. Linking Ocean Forcing and Atmospheric Interactions to Atlantic Multidecadal Variability in MPI-ESM1.2. *Geophys. Res. Lett.* **47**, e2020GL087259 (2020).
13. Mann, M. E., Steinman, B. A., Brouillette, D. J. & Miller, S. K. Multidecadal climate oscillations during the past millennium driven by volcanic forcing. *Science* **371**, 1014–1019 (2021).
14. Hu, S. & Fedorov, A. V. Indian Ocean warming can strengthen the Atlantic meridional overturning circulation. *Nat. Clim. Change* **9**, 747–751 (2019).
15. Ferster, B. S., Fedorov, A. V., Mignot, J. & Guilyardi, E. Sensitivity of the Atlantic meridional overturning circulation and climate to tropical Indian Ocean warming. *Clim. Dyn.* **57**, 2433–2451 (2021).
16. Yang, Y.-M. et al. Increased Indian Ocean-North Atlantic Ocean warming chain under greenhouse warming. *Nat. Commun.* **13**, 3978 (2022).
17. Bader, J. & Latif, M. The impact of decadal-scale Indian Ocean sea surface temperature anomalies on Sahelian rainfall and the North Atlantic Oscillation. *Geophys. Res. Lett.* **30**, 2169 (2003).
18. Fletcher, C. G. & Cassou, C. The Dynamical Influence of Separate Teleconnections from the Pacific and Indian Oceans on the Northern Annular Mode. *J. Clim.* **28**, 7985–8002 (2015).

19. Lee, S., Gong, T., Johnson, N., Feldstein, S. B. & Pollard, D. On the Possible Link between Tropical Convection and the Northern Hemisphere Arctic Surface Air Temperature Change between 1958 and 2001. *J. Clim.* **24**, 4350–4367 (2011).
20. Park, H.-S., Lee, S., Son, S.-W., Feldstein, S. B. & Kosaka, Y. The Impact of Poleward Moisture and Sensible Heat Flux on Arctic Winter Sea Ice Variability. *J. Clim.* **28**, 5030–5040 (2015).
21. Caian, M., Koenigk, T., Döscher, R. & Devasthale, A. An interannual link between Arctic sea-ice cover and the North Atlantic Oscillation. *Clim. Dyn.* **50**, 423–441 (2018).
22. Delworth, T. L. & Zeng, F. The Impact of the North Atlantic Oscillation on Climate through Its Influence on the Atlantic Meridional Overturning Circulation. *J. Clim.* **29**, 941–962 (2016).
23. Boer, G. J. et al. The Decadal Climate Prediction Project (DCPP) contribution to CMIP6. *Geosci. Model Dev.* **9**, 3751–3777 (2016).
24. Meehl, G. A. et al. Initialized Earth System prediction from subseasonal to decadal timescales. *Nat. Rev. Earth Environ.* **2**, 1–18 (2021).
25. Smith, D. M. et al. North Atlantic climate far more predictable than models imply. *Nature* **583**, 796–800 (2020).
26. Borchert, L. F. et al. Skillful decadal prediction of unforced southern European summer temperature variations. *Environ. Res. Lett.* **16**, 104017 (2021).
27. Han, W. et al. Indian Ocean Decadal Variability: A Review. *Bull. Am. Meteorol. Soc.* **95**, 1679–1703 (2014).
28. Feba, F., Ashok, K., Collins, M. & Shetye, S. R. Emerging Skill in Multi-Year Prediction of the Indian Ocean Dipole. *Front. Clim.* **3**, 736759 (2021).
29. McCarthy, G. et al. Observed interannual variability of the Atlantic meridional overturning circulation at 26.5°N. *Geophys. Res. Lett.* **39**, L19609 (2012).
30. Jackson, L. C. et al. The evolution of the North Atlantic Meridional Overturning Circulation since 1980. *Nat. Rev. Earth Environ.* **3**, 241–254 (2022).
31. Caesar, L., Rahmstorf, S., Robinson, A., Feulner, G. & Saba, V. Observed fingerprint of a weakening Atlantic Ocean overturning circulation. *Nature* **556**, 191–196 (2018).
32. Smith, D. M. et al. Robust skill of decadal climate predictions. *Npj Clim. Atmos. Sci.* **2**, 1–10 (2019).
33. Deser, C., Terray, L. & Phillips, A. S. Forced and Internal Components of Winter Air Temperature Trends over North America during the past 50 Years: Mechanisms and Implications. *J. Clim.* **29**, 2237–2258 (2016).
34. Guo, R., Deser, C., Terray, L. & Lehner, F. Human Influence on Winter Precipitation Trends (1921–2015) over North America and Eurasia Revealed by Dynamical Adjustment. *Geophys. Res. Lett.* **46**, 3426–3434 (2019).
35. Omrani, N.-E. et al. Coupled stratosphere-troposphere-Atlantic multidecadal oscillation and its importance for near-future climate projection. *Npj Clim. Atmos. Sci.* **5**, 59 (2022).
36. Huang, B. et al. Extended Reconstructed Sea Surface Temperature, Version 5 (ERSSTv5): Upgrades, Validations, and Intercomparisons. *J. Clim.* **30**, 8179–8205 (2017).
37. Rayner, N. A. et al. Global analyses of sea surface temperature, sea ice, and night marine air temperature since the late nineteenth century. *J. Geophys. Res. Atmos.* **108**, 4407 (2003).
38. Hirahara, S., Ishii, M. & Fukuda, Y. Centennial-Scale Sea Surface Temperature Analysis and Its Uncertainty. *J. Clim.* **27**, 57–75 (2014).
39. Eyring, V. et al. Overview of the Coupled Model Intercomparison Project Phase 6 (CMIP6) experimental design and organization. *Geosci. Model Dev.* **9**, 1937–1958 (2016).
40. Boucher, O. et al. Presentation and Evaluation of the IPSL-CM6A-LR Climate Model. *J. Adv. Model. Earth Syst.* **12**, e2019MS002010 (2020).
41. Hu, S. & Fedorov, A. V. Indian Ocean warming as a driver of the North Atlantic warming hole. *Nat. Commun.* **11**, 4785 (2020).
42. Nilsson, J., Ferreira, D., Schneider, T. & Wills, R. C. J. Is the Surface Salinity Difference between the Atlantic and Indo-Pacific a Signature of the Atlantic Meridional Overturning Circulation? *J. Phys. Oceanogr.* **51**, 769–787 (2021).
43. Latif, M., Sun, J., Visbeck, M. & Hadi Bordbar, M. Natural variability has dominated Atlantic Meridional Overturning Circulation since 1900. *Nat. Clim. Change* **12**, 455–460 (2022).
44. Menary, M. B. et al. Aerosol-Forced AMOC Changes in CMIP6 Historical Simulations. *Geophys. Res. Lett.* **47**, e2020GL088166 (2020).
45. Wills, R. C. J., Battisti, D. S., Armour, K. C., Schneider, T. & Deser, C. Pattern Recognition Methods to Separate Forced Responses from Internal Variability in Climate Model Ensembles and Observations. *J. Clim.* **33**, 8693–8719 (2020).
46. Bellucci, A., Mattei, D., Ruggieri, P. & Famooss Paolini, L. Intermittent Behavior in the AMOC-AMV Relationship. *Geophys. Res. Lett.* **49**, e2022GL098771 (2022).
47. Scaife, A. A. & Smith, D. A signal-to-noise paradox in climate science. *Npj Clim. Atmos. Sci.* **1**, 28 (2018).
48. Xia, F., Zuo, J., Sun, C. & Liu, A. The Atlantic Meridional Mode and Associated Wind–SST Relationship in the CMIP6 Models. *Atmosphere* **14**, 359 (2023).
49. Domeisen, D. I. V. et al. Seasonal Predictability over Europe Arising from El Niño and Stratospheric Variability in the MPI-ESM Seasonal Prediction System. *J. Clim.* **28**, 256–271 (2015).
50. Zanchettin, D. et al. A decadally delayed response of the tropical Pacific to Atlantic multidecadal variability. *Geophys. Res. Lett.* **43**, 784–792 (2016).
51. Vellinga, M. & Wu, P. Low-Latitude Freshwater Influence on Centennial Variability of the Atlantic Thermohaline Circulation. *J. Clim.* **17**, 4498–4511 (2004).
52. Ba, J. et al. A multi-model comparison of Atlantic multidecadal variability. *Clim. Dyn.* **43**, 2333–2348 (2014).
53. Brunner, L. et al. Reduced global warming from CMIP6 projections when weighting models by performance and independence. *Earth Syst. Dyn.* **11**, 995–1012 (2020).
54. Latif, M. et al. Reconstructing, Monitoring, and Predicting Multidecadal-Scale Changes in the North Atlantic Thermohaline Circulation with Sea Surface Temperature. *J. Clim.* **17**, 1605–1614 (2004).
55. Sévellec, F., Fedorov, A. V. & Liu, W. Arctic sea-ice decline weakens the Atlantic Meridional Overturning Circulation. *Nat. Clim. Change* **7**, 604–610 (2017).

ACKNOWLEDGEMENTS

This research is supported by the ARCHANGE project of the "Make our planet great again" program (ANR-18-MPGA-0001, France). Additional support is provided to AVF by NSF (AGS-2053096) and DOE (DE-SC0024186). JM is also supported by the ANR-19-JPOC-003 JPI climate/JPI ocean ROADMAP project. This study benefited from the ESPRI (Ensemble de Services Pour la Recherche l'IPSL) computing and data centre (https://mesocentre.ipsl.fr) which is supported by CNRS, Sorbonne University, Ecole Polytechnique and CNES and through national and international grants. LFB received funding by the Deutsche Forschungsgemeinschaft (DFG, German Research Foundation) under Germany's Excellence Strategy, EXC 2037 "Climate, Climatic Change and Society" CLICCS (project no. 390683824), as a contribution to the Center for Earth System Research and Sustainability (CEN) of Universität Hamburg. LFB and MM are also supported through the ANR-TREMPLIN ERC Project HARMONY, Grant Agreement Number ANR-20-ERC9-0001. We acknowledge the World Climate Research Programme, which, through its Working Group on Coupled Modelling, coordinated and promoted CMIP6. We thank the climate modeling groups for producing and making available their model output, the Earth System Grid Federation (ESGF) for archiving the data and providing access, and the multiple funding agencies who support CMIP6 and ESGF.

AUTHOR CONTRIBUTIONS

B.S.F. and L.F.B. designed the experimental methods. B.S.F. ran most of the analyses and processed the results. The motivation of the atmospheric teleconnection derives from previous work by A.V.F. and B.S.F. L.F.B. and B.S.F. wrote the initial paper. All authors analyzed the results and contributed to editing the paper.

COMPETING INTERESTS

The authors declare no competing interests.

ADDITIONAL INFORMATION

Supplementary information The online version contains supplementary material available at https://doi.org/10.1038/s41612-023-00489-x.

Correspondence and requests for materials should be addressed to Brady S. Ferster or Leonard F. Borchert.

Reprints and permission information is available at http://www.nature.com/reprints

Publisher's note Springer Nature remains neutral with regard to jurisdictional claims in published maps and institutional affiliations.